6th Quarter Research Performance Progress Report

Project Title:	Pore Scale Control of Gas and Fluid Transport at Shale Matrix-Fracture Interfaces
Project Period:	10/01/16 – 09/30/18
Reporting Period:	1/1/18 – 3/31/18
Submission Date:	5/15/2018
Recipient:	SLAC National Accelerator Laboratory
Recipient DUNS #:	00-921-4214
Address:	2575 Sand Hill Road, MS 69 Menlo Park, CA 94025
Website (if available)	www-ssrl.slac.stanford.edu
Award Number:	FWP 100211
Awarding Agency:	NETL

Principal Investigator:	Dr. John Bargar Senior Staff Scientist SLAC National Accelerator Laboratory Phone: 650-926-4949 Email: bargar@slac.stanford.edu
Co-Principal Investigators:	Dr. Gordon E. Brown, Jr. Dr. Kate Maher Dr. Anthony Kovscek Dr. Mark Zoback
NETL Project Manager:	David Cercone

TABLE OF CONTENTS

1. EXECUTIVE SUMMARY

Hydraulic stimulation of unconventional reservoirs has transformed the U.S. energy economy and provided powerful technical capabilities to implement national energy policy, while reducing worldwide reliance on less environmentally friendly fossil fuels [1]. In spite of these achievements, unconventional production remains highly inefficient, with much of the resource remaining in place. This project is improving fundamental knowledge of two important sources of inefficiency: (i) scale precipitation, which clogs fractures and matrix porosity, and (ii) the chemistry and microstructure of fracture-matrix interfaces, which are the gateways through which gas and oil must flow in order to be collected from the largely inaccessible reserve of hydrocarbons within the shale matrix (**Figure 1**).

Fluids injected during unconventional stimulation react strongly with shale, dissolving and mechanically weakening fractures and proppant alike, driving scale precipitation, and initiating a cascade of organic-mediated, oxidation-reduction geochemical reactions. These reactions are of intense interest because of their potential to reduce permeability and inhibit production. Importantly, they also offer a means to adaptively tailor geochemical reactions and matrix permeability in specific and desired fashions, to selectively arrest or accelerate scale precipitation, and to initiate and control chemical and physical processes that could be used to liberate more resource from the matrix. In order to prevent scale precipitation and improve control of fluid and gas flow, a commanding grasp of the geochemical factors that govern 'keystone' reactions such as barite and iron oxide precipitation and control of matrix access is critical.

The largely inaccessible interior of the shale matrix is a 'frontier' research focus because it is the largest mostly untapped reservoir of the desired resources. For this reason, *even a small fractional increase in production from the matrix has the potential to deliver large absolute increases in production*. For example, increasing oil production from matrix from 5% to 10% would *double* production in an average well. The low permeability and diffusivity of the shale matrix is in many cases the most significant impediment to production. It is therefore paramount to understand chemical, microstructural, and permeability alteration of the *altered zone* through which oil and gas flow.

Knowledge gaps: Shale reservoirs are highly complex physically and chemically. The majority of chemical additives used in hydraulic fracturing were developed based on research findings from conventional oil/gas systems. Due to the difference in industrial processes and source material, a different way of thinking about unconventional systems is needed. As a community, we lack understanding of the fundamental geochemical and kinetic parameters that govern precipitation of ubiquitous scale phases such as barite in unconventional reservoirs during and following stimulation. We also lack basic physical-chemical numerical models to predict gas and fluid transport across the altered zone.

This project is conducting fundamental research to address two crucial and interrelated reservoir performance needs that provide the potential to deliver significant increases in efficiency:

(i) Reducing scale precipitation through better understanding and control of fundamental geochemical and kinetic factors; and

(ii) Improving microscale knowledge of the fracture-matrix interface required to develop chemical/physical manipulation approaches that can access the resource in the matrix.

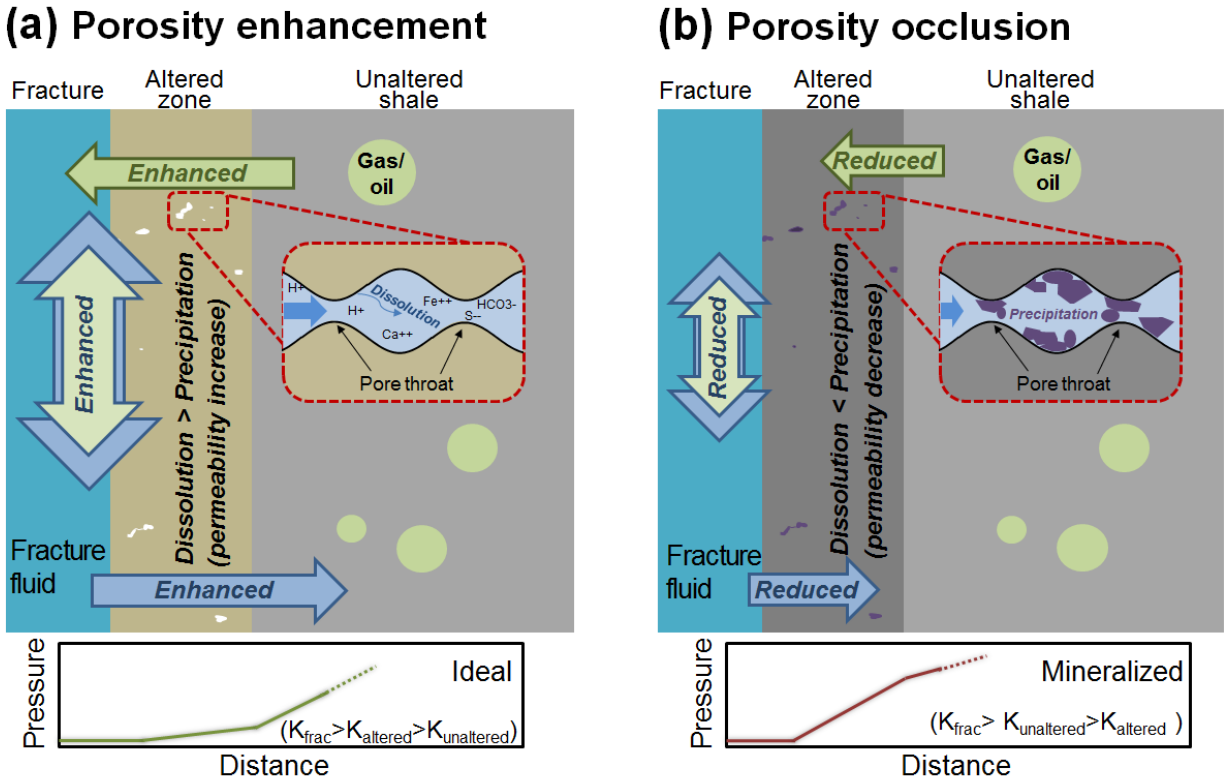

Figure 1: Conceptual model illustrating the altered zone at shale-fluid interfaces and the possible effects of dissolution and precipitation reactions on gas and water flow through the altered fracture surface. As seen in the left panel, when shales react with acidic solutions, increased porosity facilitates transport into the shale matrix, resulting in a concave up pressure gradient and enhanced recovery. Precipitation of secondary minerals in the altered zone (right panel) decreases permeability, leading to a concave down, and less ideal, pressure gradient.

As described herein, the work reported in the current quarter is helping to emphasize three important points:

- *"Low reactivity" shale matrices are, in fact, quite reactive*. When present in fracture fluid, oxygen penetrates rapidly (*i.e.*, within the typical 3 to 6 week duration of shut-in periods during stimulation) into shale interfaces, even when micro-fractures are not present. The reaction depth of secondary Fe(III) precipitation in the altered zone is 200 to 300 μm for both Pennsylvania Marcellus and Eagle Ford shales. This reactivity helps to explain the extensive alteration that develops when micro-fractures are present.
- *Manipulating the rates of dissolution and scale precipitation reactions provides a path to engineer the permeability of the altered zone at shale-fluid interfaces*. Our work over the past two years has shown that the rates of dissolution and scale precipitation are highly sensitive to pH, ionic strength, and the presence of dissolved solutes such as sulfate. Using this knowledge, it should be possible to design and test chemical-based methods to engineer altered zone permeability by manipulating the rates of dissolution and precipitation reactions.

- Only a small amount of bitumen is required to dramatically accelerate Fe(II) oxidation by oxygen at low pH during stimulation. Virtually all economically important shales are relatively enriched in organics. Therefore, *organic-promoted oxidation pathways will control Fe(II) oxidation and scale formation in all unconventional reservoirs.*

2. GOALS AND OBJECTIVES

The overarching goal of this project is to discover new fundamental knowledge about: (i) geochemical and kinetic controls over secondary mineral precipitation; and (ii) fluid-induced chemical/microstructural alterations to shale interfaces and their impacts on permeability and gas/fluid transport. We are accomplishing these goals through a suite of activities that integrate synchrotron-based imaging and CT methods, electron microscopy, permeability measurements, and geochemical and reactive transport modeling. This approach is allowing us to associate pore- and fracture-scale geochemical processes to resultant changes in transport properties.

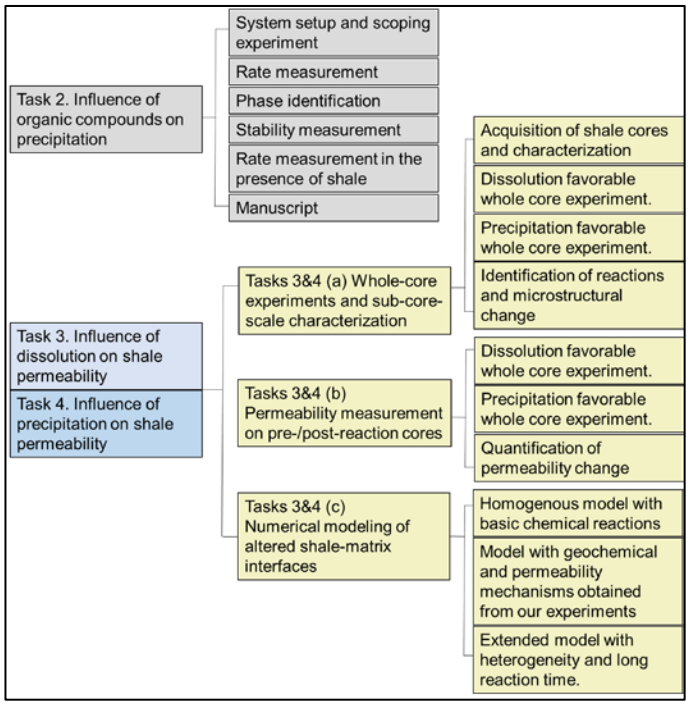

Figure 2. Structure of this report and the relation to PMP tasks. Task 1 (not illustrated) is the program management activity.

Task 1 encompasses project management activities. The three scientific tasks defined in our project management plan are (**Figure 2**): **Task 2**: Characterizing the influence of dissolved organic compounds, pH, and ionic strength on barite scale precipitation. In contrast, **Tasks 3 and 4** are focused on characterizing and modeling the chemical/microstructural alteration of shale-fracture interfaces and the impact of this alteration on gas transport. **Task 3** is nominally oriented toward porosity generation within the altered layer ('dissolution favorable' conditions, Figure 3), whereas **Task 4** is focused on secondary mineral precipitation within the altered layer

('precipitation favorable' conditions). These two chemical processes are interrelated (dissolution leads to precipitation), and the work flows for subtasks 3 and 4 are similar. Consequently, Task 3 and 4 efforts have been merged and are reported in section 3 (this section) as "**Task 3&4**". The merged work flow for **Task 3&4** self-organizes into 3 primary activities: (a) Chemical reactions and sub-core-scale geochemical characterization; (b) permeability measurement, which requires whole-core characterization using core-flood approaches; and (c) numerical modeling of altered shale-matrix interfaces. Results for each are presented separately later in this section. Effort for **Task 3&4** in Year 1 has focused on activities (a) and (b), whereas numerical modeling will be a more significant focus in Year 2.

3. TECHNICAL HIGHLIGHTS

Task-by-task highlights of accomplishments in Quarter 6:

Task 1

1. The approved project management plan is being implemented with each goal being completed on-time.
2. Teleconference and in-person meetings with research scientists at NETL are conducted as needed.

Task 2. Effects of dissolved organic matter on the precipitation and stability of secondary mineral phases

3. An initial manuscript draft is complete and on-schedule. There are no new experimental results to report for this task, as planned in the Project Management Plan.

Tasks 3 & 4 (a) Fundamental precipitation and dissolution reactions controlling porosity

4. The reaction depths of Fe(III) precipitation into the shale matrices were obtained from multi-energy μ-XRF mapping at SSRL beamline 2-3.

Tasks 3 & 4 (b) Measuring permeability alteration

5. Permeability was measured from post-reaction Marcellus core samples, and the results support the findings of earlier work.
6. Permeability was measured from pre- and post-reaction of Eagle Ford core samples.
7. SEM with EDS measurements were performed on the reacted cores and analyzed to determine if variations in shale permeability (Marcellus vs Eagle Ford) are due to mineral alteration of shale matrix caused by fracture fluid reaction as outlined in our overarching model (Figure 1).

Tasks 3 & 4 (c) Numerical simulation of secondary porosity generation and scale precipitation during shale-fluid interactions

8. Kinetic information was obtained from modeling of barite precipitation experiments.
9. Kinetic information was obtained from modeling of bitumen-catalyzed Fe(II) oxidation experiments.

Details of task progress:

Task 2: Effects of dissolved organic matter on the precipitation and stability of secondary mineral phases

Barite ($BaSO_4$) scale precipitation is a prime concern in nearly all hydraulic fracturing systems, both in shale bodies and in piping. Because of its ubiquitous presence and low solubility, barite tends to be over-saturated. Barite is added to drilling muds (DM) at high concentrations (> 10 g/kg) in order to increase the density of the muds and aid in the drilling process [2-4]. Even though some operators attempt to remove as much of the DM as possible, significant amounts of DM are imbedded in the rock during the drilling process and remain. This leftover DM can then react with the initial hydrochloric acid slug (~15%) injected down bore hole to clean up perforations in the bore casing and to help clean out the drilling mud. In comparison to the drilling mud, barium concentrations native to the shale host rock are lower, typically ≤ 1 g/kg in the solid [5]. The high volume/pressure of the injection fluid and the low pH (~ pH 0), result in a high probability of dissolving and mobilizing Ba from the DM and forcing it into the newly formed fractures as well as the shale matrix itself. This introduction of significant quantities of Ba^{2+} and SO_4^{2-}, including that leached from the shale itself, will lead to scale production, clogging of newly developed secondary porosity, and overall attenuation of permeability.

The scope of this task includes investigating the effects of various classes of added and natural organics found in hydraulic fracturing systems, including fracture fluid additives (biocides, breakers, crosslinkers, friction reducers, scale inhibitor, Fe-control, corrosion inhibitor, and gellants), as well as those present in shale (both formation and produced waters). Major questions being addressed by this task are, how do variations in pH, ionic strength, dissolved organic compounds, and mineral surface area impact Ba release into hydraulic fracturing systems and subsequent barite scale precipitation?

Progress in quarter 6:

An initial draft of the manuscript for this task is complete

Results: No new results to report.

Planned Experiments: No new experiments are planned.

Table 1: Task 2 objectives for Quarter 6

Goal	Status
Initial draft of manuscript	Completed

Manuscript plans: An initial manuscript draft detailing the effect of various organics on the precipitation of barite at various ionic strengths is completed. A working title for this manuscript is: Organic and inorganic controls on barite precipitation in hydraulic fracturing systems. Additionally, an extended abstract has been accepted for the URTeC conference this summer in

Houston, TX entitled: Barium Sources in Hydraulic Fracturing Systems and Chemical Controls on its Release into Solution.

Task 3&4 (a): Fundamental precipitation and dissolution reactions controlling porosity

Upon exposure to acidic fracture fluid, shale matrices experience mineral dissolution, which leads to an increase in dissolved mineral forming solutes in solution and a slow rise in pH. These changes in solution chemistry create conditions favorable for secondary mineral precipitation (*cf.*, **Figure 1**). Because of this, there are two major competing processes (dissolution and mineral precipitation) that can alter porosity, diffusivity, and permeability of the matrices, resulting in either an enhancement or reduction in gas/oil production.

In this section (**Task 3&4(a)**) we reacted whole core sections with fracture fluid and characterized them with μ-x-ray CT and synchrotron μ-XRF chemical mapping to determine porosity changes, alteration zone thickness, primary minerals dissolving (e.g., carbonate and pyrite), and precipitating phases (e.g., Fe/Al oxides and Ca/Ba sulfate). These measurements allow for identifying the spatial distribution of these reactions within the shale pore structure. A related task (**Task 3&4 (b)**), focuses on reaction-induced permeability alterations of the shale matrix using laboratory-based porosity and permeability measurements and connected back to this task to relate microstructural changes to permeability. In **Task 3&4 (c)**, secondary porosity generation and mineral precipitation are numerically simulated in order to understand the mechanisms of shale-fluid interactions and predict future shale alteration based on initial shale mineralogy.

Table 2: Objectives in Tasks 3&4 (a) for Quarter 6.

Goal	Status
Reconstruct μ–CT data for reacted and unreacted cores obtained in December	Complete
Collect and analyze multi-energy synchrotron μ-XRF maps of Fe for post-reaction core cross sections	Complete

Progress in Quarter 6:

In earlier quarters, we have mapped the depths of reaction fronts into shale matrices for barite scale precipitation and sulfur oxidation. Because oil/gas shales can contain high concentrations of calcite and pyrite which can have large impacts on porosity/permeability, the length scale of reaction zones for carbonate dissolution and iron oxidation needs to be determined. This can be determined by locating secondary porosity and Fe(III)-(oxyhydr)oxide formation close to the shale-fluid interfaces. In this quarter, efforts have been made to characterize secondary porosity from synchrotron μ-CT data and to locate Fe(III)-(oxyhydr)oxide precipitation using multi-energy synchrotron μ-XRF maps.

Results in Quarter 6:

Because of the heterogeneity in shale matrices, collected μ-CT data did not have enough resolution in order to show observable changes in secondary porosity except for the Pennsylvania Marcellus shown in **Figure 7** in **Quarter 5 Report**. More detailed data analyses will be carried out on this CT data set, and we also attempt to characterize secondary porosity using SEM-BSE imaging. The following results focus on multi-energy synchrotron XRF Fe mapping.

Iron multi-energy XRF maps were acquired at SSRL beamline 2-3 in January, 2018. The multi-energy maps allow us to map the spatial distribution of pyrite and Fe(III)-(oxyhydr)oxides. The cores for multi-energy map collection were Pennsylvania Marcellus and Eagle Ford reacted with synthetic fracture fluid only (Condition 1) or with synthetic fracture fluid that contains 2 mM $BaCl_2$ and 0.06 mM Na_2SO_4 (Condition 2) to promote barite precipitation. Results (**Figure 3**) show that Fe(III)-(oxyhydr)oxides precipitated about 200 – 300 μm into the matrices for both Pennsylvania Marcellus and Eagle Ford, with Eagle Ford slightly deeper into the matrix. The Fe(III)-rich rims for duplicate samples were thicker, because duplicate experiments were run with a larger headspace (1 bar of air and 76 bar of N_2) above reaction solution in the sealed reactors, where more oxygen is available to oxidize Fe. New York Marcellus did not show a rim of Fe(III) secondary precipitation due to the lack of connected porosity (such as micro cracks) that leads reaction into the matrix, and therefore is not shown here.

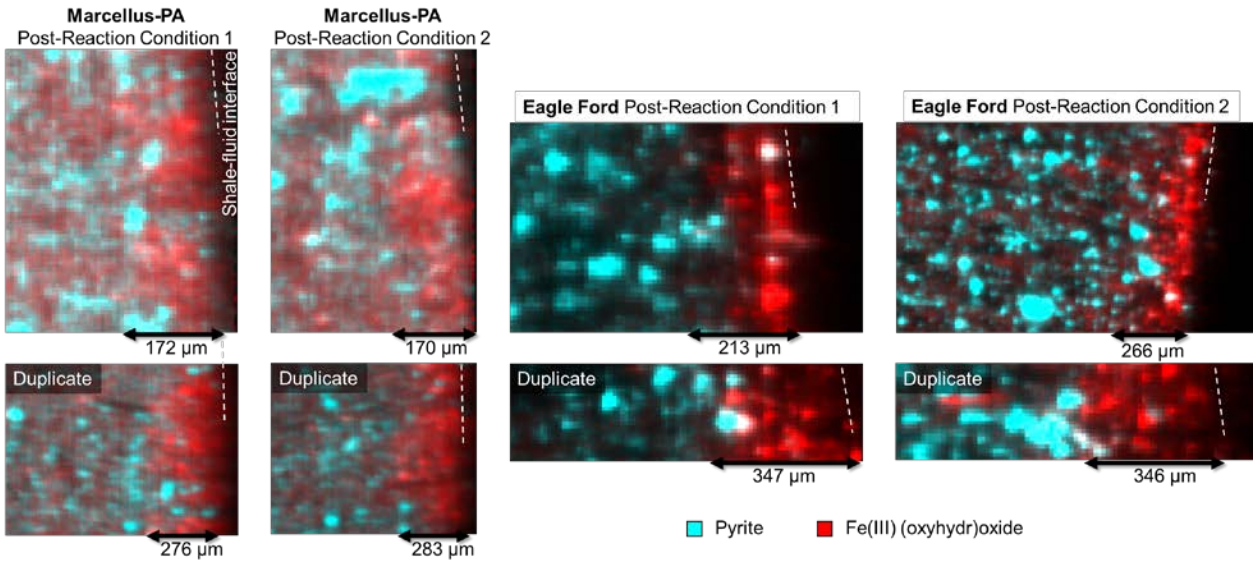

Figure 3. Pyrite and Fe(III)-(oxyhydr)oxide spatial distribution maps on Pennsylvania Marcellus and Eagle Ford cross sections after reaction with fracture fluid. Step size is 15 μm. Shale core surfaces are on the right of the maps as indicated by dotted lines. Pyrite is shown in cyan and Fe(III)-(oxyhydr)oxide is shown in red. The color intensities are scaled for each individual map (i.e., absolution color intensities vary from map to map) to show the spatial distribution clearly. Iron (III)-rich precipitates are observed close to the shale-fluid interfaces, where pyrite has been dissolved. Condition 1 refers to reactions in fracture fluid, and Condition 2 refers to reactions in fracture fluid with additional Ba^{2+} and SO_4^{2-} to form barite scale.

Comparing results in the matrices of Marcellus-NY and Marcellus-PA, it is clear that connected pores are important in leading chemical reactions into the matrix. Such a result is consistent with sulfur oxidation in earlier reports, where Marcellus-NY showed low chemical reactivity because it does not have micro cracks. It is also noted that for shales with micro cracks, namely Marcellus-PA and Eagle Ford, the Fe(III) precipitation layer is not confined to micro cracks, but is fairly uniform along the shale surface, indicating that connected pores other than micro cracks are also important in determining chemical reactivity of the shale matrix.

Interestingly, in Marcellus-PA, the reaction zone depth of Fe(II) oxidation (200-300 μm) is much less than S oxidation (≥ 5 mm) reaction depth. This is expected, because for the low carbonate Marcellus, pH of the pore water was low due to lack of carbonate dissolution. The low pH retarded Fe(II) oxidation rate [6], allowing dissolved oxygen to migrate deeper into the matrix to oxidize S. Conversely, in the carbonate-rich Eagle Ford, the pH of the pore water was near neutral, accelerating Fe oxidation which consumed much of the dissolved oxygen, leaving limited oxygen to further oxidize S deeper in the matrix. With the rim of Fe(III) secondary precipitation filling the pores and pore throats, gas/oil transport across the shale-fracture interface may be reduced, impairing recovery efficiency.

Planned Experiments in the next quarter:

- Further analyze μ-CT data to quantify reaction depths of carbonate dissolution.
- Collect SEM-BSE images on cross sections to help quantify reaction depths of carbonate dissolution.
- Complete URTeC 2018 extended abstract
- Complete initial draft of manuscript regarding shale matrix reactions

Task 3&4 (b): Measuring permeability alteration induced by fracture fluid reaction

For oil/gas production, alteration of the fracture surface microstructure modifies matrix permeability and thus production. In this section, we are conducting permeability measurements before and after dissolution-favorable and precipitation-favorable experiments, followed by microscale characterization using both scanning electron microscopy (SEM) imaging coupled with energy dispersive spectroscopy (EDS) analysis. These measurements complement μ-CT and μ-XRF measurements described in Task 3&4 (a) in this report and earlier quarterly reports. These experiments give us insights showing direct relation of fracture fluid reaction impact on permeability.

Progress in Quarter 6:

Permeability measurements of two shale samples of varying carbonate concentrations were performed before and after reaction with acidic hydraulic fracturing fluid. Following permeability measurements, samples were analyzed using SEM imaging and Energy Dispersive Spectroscopy (EDS) to image changes to sample texture along with elemental speciation to support results of the permeability measurements.

The shale reactions were performed inside a batch reactor with the dissolution-favored synthetic fracture fluid (initial pH=2.0) at 77bar and 80°C for 6 days, with added $BaCl_2$ and Na_2SO_4 salts in place of barite-rich drilling mud to promote barite precipitation. A list of the synthetic fracture fluid composition is listed in Table 3.1

Table 3: Objectives in Tasks 3&4 (b) for Quarter 6.

Goal	Status
Permeability measurements of post-reaction Marcellus core collected.	Complete
Permeability Measurements of pre- and post-reaction Eagle Ford core collected.	Complete
SEM Imaging and EDS Analysis of shale matrix alteration induced by fracture fluid reaction.	Complete

Results in Quarter 6:

For the Marcellus microcore (**Figure 4a**), a decrease in measured permeability was observed for post-reaction measurements (0.040, 0.027, 0.022, 0.015 μdarcy) compared to pre-reaction measurements (0.049, 0.032, 0.025, 0.019 μdarcy) at increasing pore pressures (200, 400, 800, 2000 psi), respectively. Conversely, the Eagle Ford microcore (**Figure 4b**) had the opposite trend in measured permeability, showing a large increase for post-reaction measurements (3.361, 3.059, 2.799, 0.767 μdarcy) compared to pre-reaction measurements (0.431, 0.342, 0.254, 0.088 μdarcy) at similar pore pressure steps.

We extend our findings to compute the intrinsic permeability of each sample using Klinkenberg analysis. Following Klinkenberg's equation [**7**], a linear fit is observed between inverse pore pressure and measured permeability such that intrinsic permeability is equal to the y-intercept.

Table 3.1. Synthetic fracture fluid chemistry. Based on NETL's Greene County, PA, Well E.

Ingredient	Purpose	Percentage of Ingredient (by mass)
Water	Base Fluid	99.783%
Ethylene Glycol	Scale Inhibitor, Iron Control, Breaker	0.021%
Kerosene	Friction Reducer	0.024%
Guar Gum	Dry Gellant	0.029%
2-Ethyl hexanol	Corrosion Inhibitor for Acid	0.0005%
Glycol ether	Corrosion Inhibitor for Acid	0.0002%
Polyethylene glycol	Biocide	0.020%
Hydrochloric acid	Acid	0.122%

$$K_{measured} = K_{\infty}\left(1 + \frac{K_b}{\overline{Pp}}\right)$$

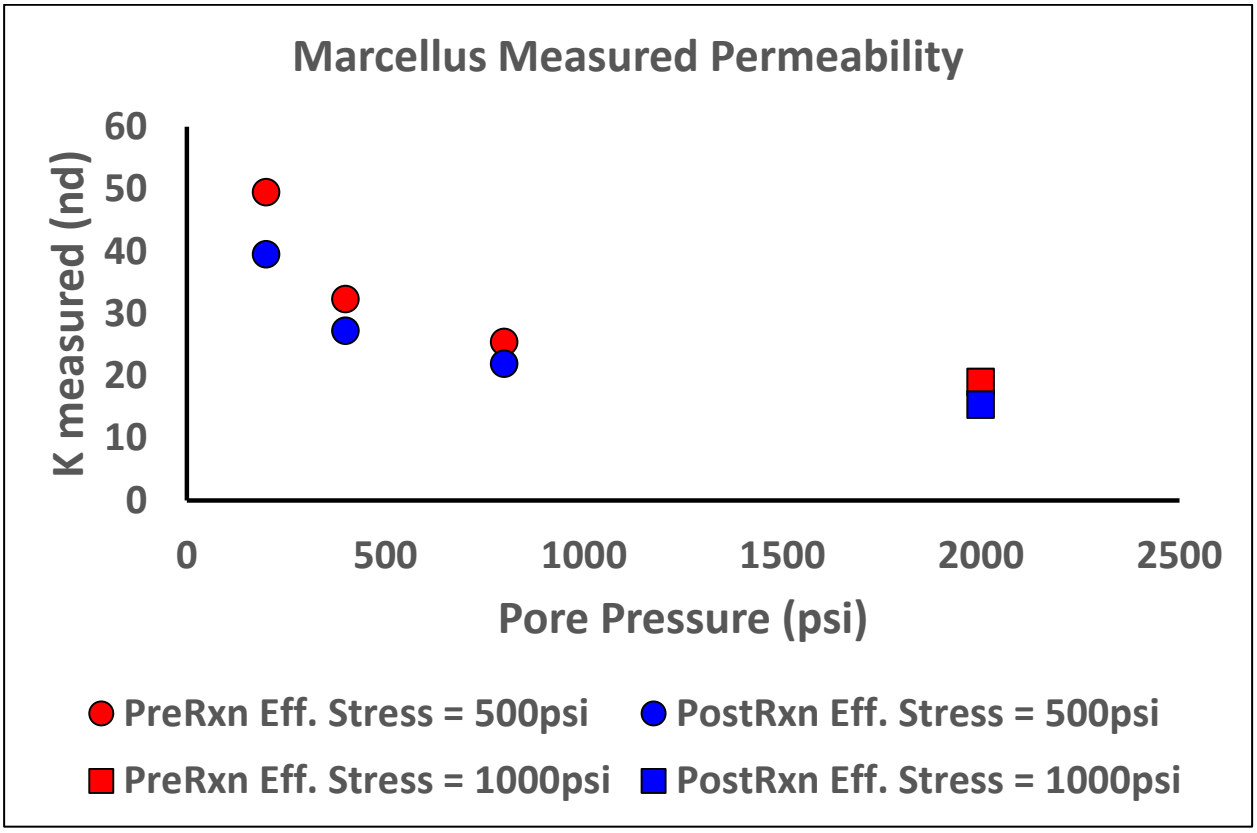

Figure 4a. Measured Permeability for pre- and post-reaction Marcellus sample. Reaction conditions were set at 77bar and 80°C for 6 days, with added $BaCl_2$ and Na_2SO_4 salts in place of barite-rich drilling mud to promote barite precipitation. Pulse permeability measurements were acquired at incrementally increasing pore pressures (200psi, 400psi, 800psi) while maintaining an effective pressure=500psi in order to calculate the intrinsic permeability from Klinkenberg analysis. An additional permeability measurement was collected at pore pressure=2000psi and effective pressure=1000psi to replicate relative reservoir production conditions (points with square markers).

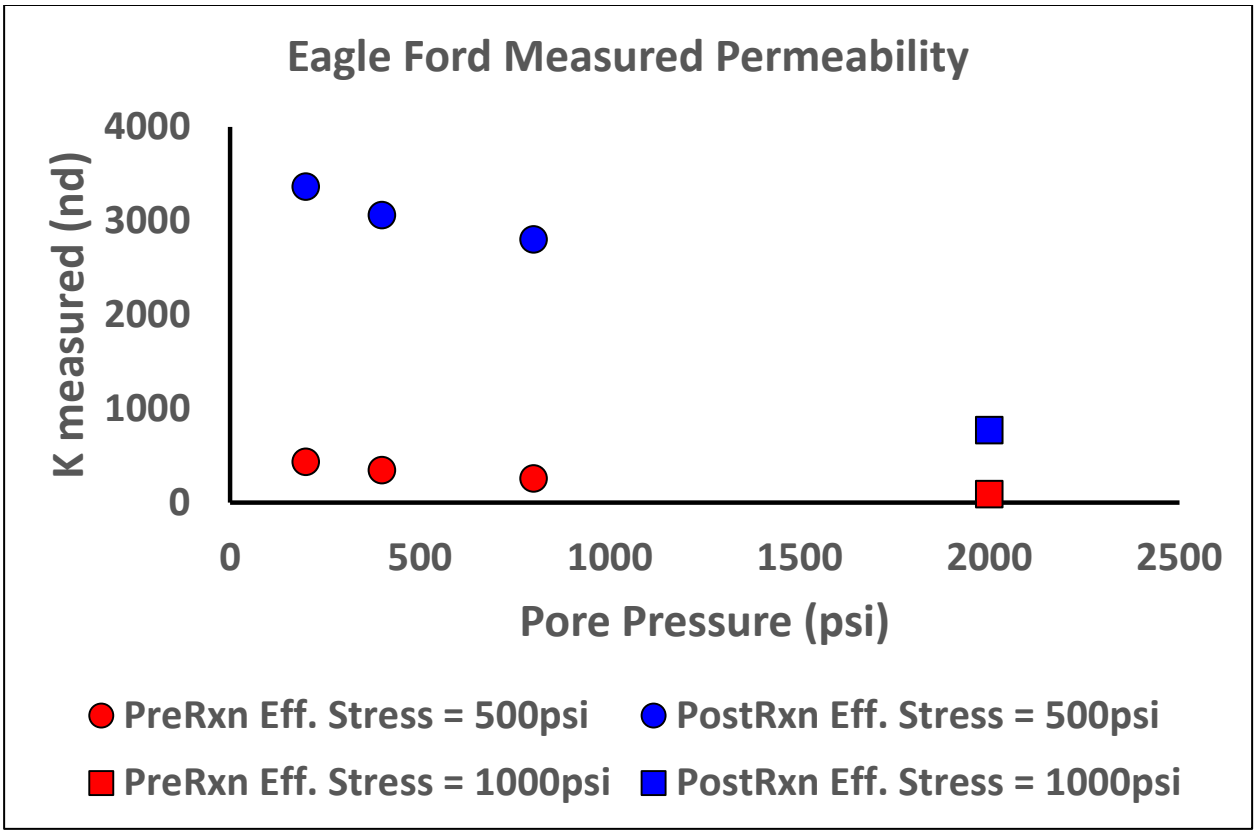

Figure 4b. Measured Permeability for pre- and post-reaction Eagle Ford sample. Reaction conditions were set at 77bar and 80°C for 6 days, with added $BaCl_2$ and Na_2SO_4 salts in place of barite-rich drilling mud to promote barite precipitation. Pulse permeability measurements were acquired at incrementally increasing pore pressures (200psi, 400psi, 800psi) while maintaining an effective pressure=500psi in order to calculate the intrinsic permeability from Klinkenberg analysis. An additional permeability measurement was collected at pore pressure=2000psi and effective pressure=1000psi to replicate relative reservoir production conditions. (points with square markers).

By utilizing the first 3 pulse-decay measurements set at increasing pore pressures 200psi, 400psi, 800psi, with a constant effective pressure of 500psi, we calculate the intrinsic permeability (K_∞) for each sample as shown in **Figure 5a and 5b**. We observe the same decreasing trend for intrinsic permeability going from 0.017 µdarcy to 0.015 µdarcy for the Marcellus microcore (**Figure 5a**) and an increasing trend in intrinsic permeability, by an order of magnitude, going from 0.209 µdarcy to 2.648 µdarcy for the Eagle Ford microcore (**Figure 5b**). This highlights a 6.5% reduction in Marcellus permeability and a 1000% increase in Eagle Ford permeability post-reaction with fracture fluid. These findings would at first glance appear to contradict our previous results showing that barite scale precipitates *more* extensively in the Eagle Ford cores than in Marcellus cores (5^{th} Quarter report, Figure 5; 2017 Annual Report, Figure 10). It is thus necessary to look for a nuanced explanation to explain the sharply increased permeability in Eagle Ford cores.

One potential explanation for this contrast is that mineral dissolution in the Eagle Ford shale continued to enhance permeability even while barite precipitation was occurring. In contrast,

mineral precipitation in Marcellus shale appears to have reduced overall permeability. To determine whether mineral dissolution/precipitation is occurring on a large scale in these samples we investigated the micro-scale shale matrix alterations occurring on the surface of each sample using SEM imaging with EDS analysis.

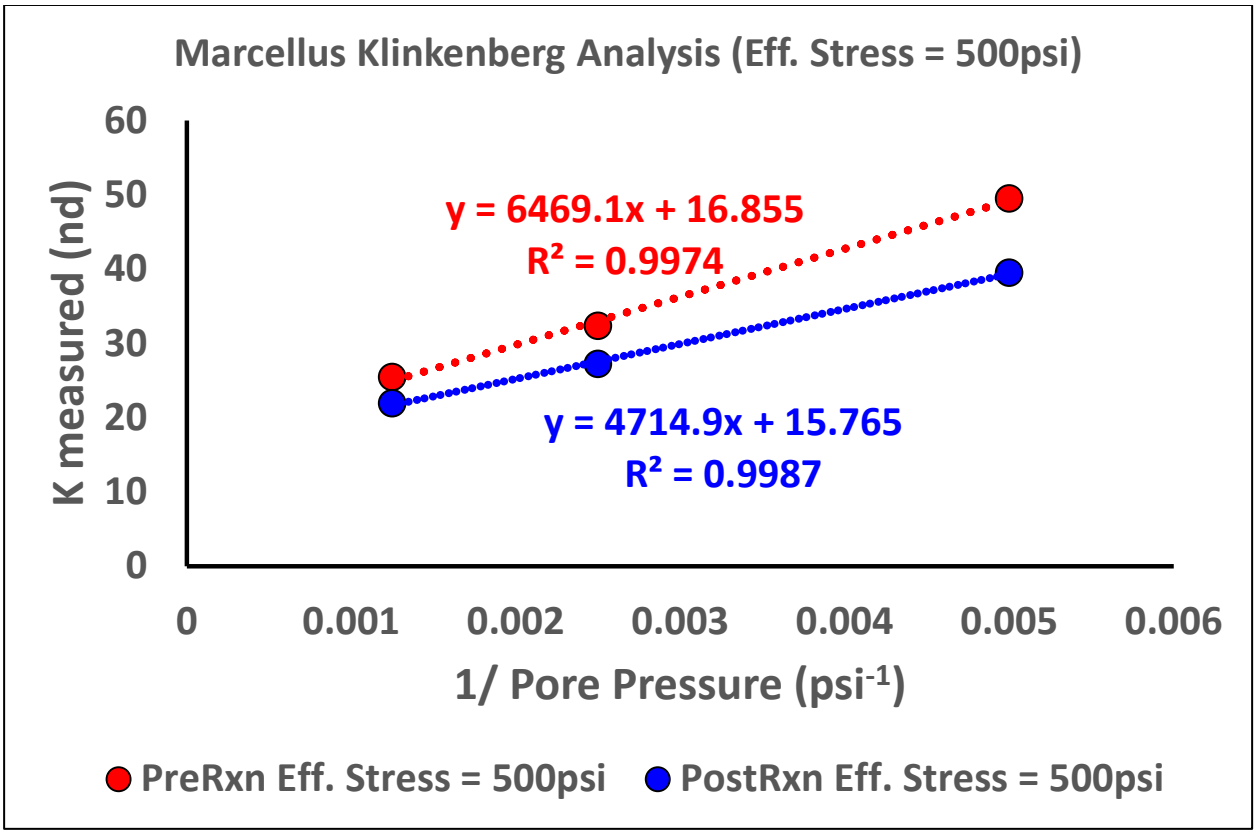

Figure 5a. Klinkenberg analysis for pre- and post-reaction Marcellus sample done for varying pore pressures at constant effect pressure=500psi. From the fitted trend line, the y-intercept is the intrinsic permeability (K_∞). We show the intrinsic permeability of the Marcellus sample reduced slightly post-reaction to fracture fluid.

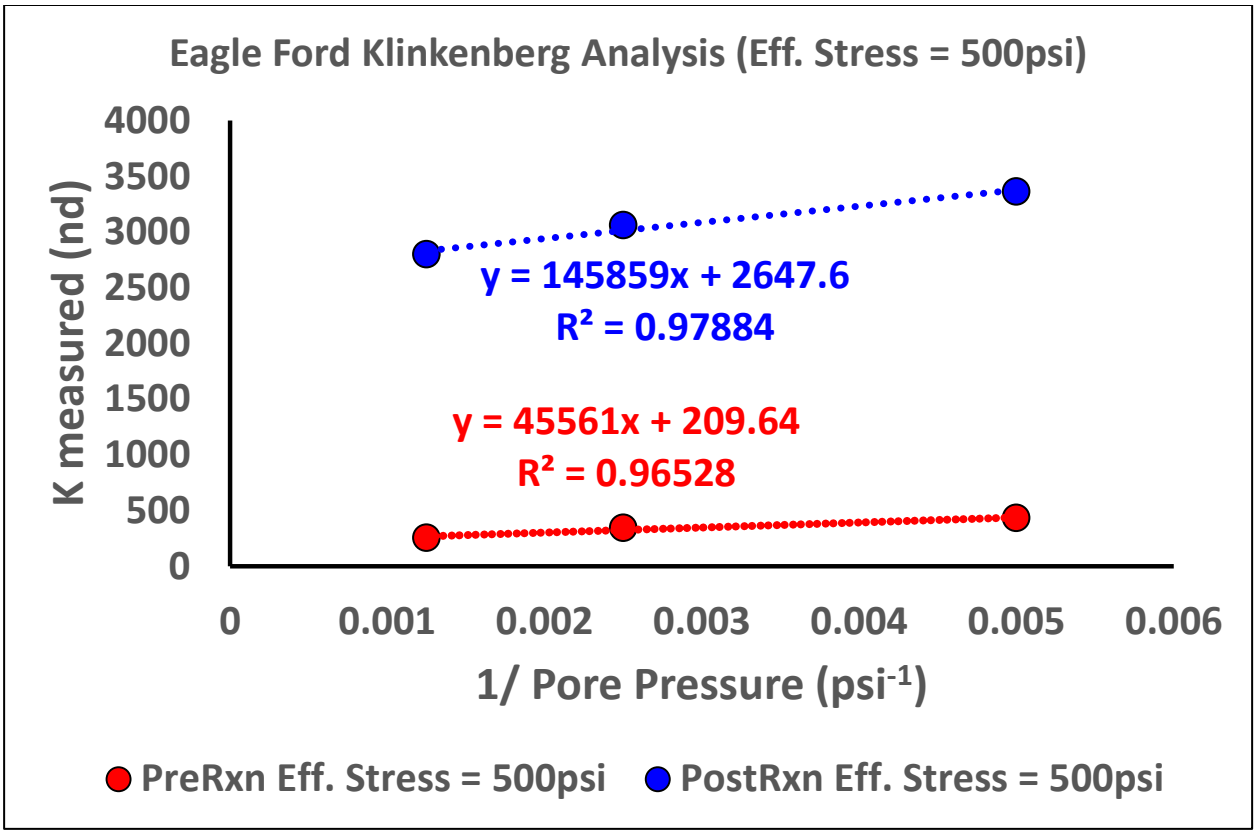

Figure 5b. Klinkenberg analysis for pre- and post-reaction Eagle Ford sample done for varying pore pressures at constant effect pressure=500psi. From the fitted trend line, the y-intercept is the intrinsic permeability (K_∞). We show the intrinsic permeability of the Eagle Ford shows an increase in intrinsic permeability by an order of magnitude post-reaction.

High-resolution SEM images were collected on a FEI Magellan 400 XHR, linked with a Bruker Quantax XFlash energy dispersive spectra (EDS) detector. Images were acquired at fiducial points along the microcore shale surface that could help facilitate alignment of pre- and post-reaction images and thus to allow us to see if surface alteration occurred as a result of either mineral dissolution or precipitation within the shale matrix. All SEM images acquired are backscattered electron images using a concentric backscatter detector with inner a-ring attached (CBS-a), to provide the best elemental contrast and remove any topographical discrepancy across the sample surface. All EDS measurements were performed using the following settings: beam voltage 15kV, beam current 13nA, at a magnification of 150x-200x in order to include as much surface area into the analysis.

Qualitative elemental maps of the EDS data were produced using Quantax Esprit 2.1 software. The object classification images are based on a combination of both principal component analysis and cluster analysis of neighboring points from EDS data. We classify the objects into the following phases: (1) Silicate- or Shale Matrix (green), (2) Organic Matter (blue), (3) Clay (pink), (4) Carbonate (cyan), (5) Pyrite (red), (6) Silicates (magenta), (7) Barite (yellow), and the remainder black clusters represent pore space.

Figures 6 and 7 show sequential images highlighting changes pre- (top row) and post-reaction (bottom row) with the fracture fluid. A backscattered SEM image with CBS-a detector

(left) shows the textural changes along the shale matrix and micro-cracks, while the object classification image shows the mineralogy identified from clusters analysis of EDS data (middle), and the final column (right) combines both images to get a composite image. We focused on the occurrence of barite precipitation by including barite into the object classification by using the acquired barium and sulfur elemental maps.

For the Marcellus (**Figure 6**) pre-reaction sample (top row), we note a clay-rich matrix (green), clay minerals (magenta) and pyrite (red) dispersed across the matrix, and a large micro-crack filled with organic matter (blue). Comparing it to the post-reaction images (bottom row), no secondary porosity generation is evident across the backscattered image (bottom left), whereas the micro-cracks are filled with a high contrast mineral. From the object classification image (bottom middle), we identify the bright mineral as barite (yellow) in the form of minor precipitation dispersed across the matrix with the majority of the barite deposited in the micro-cracks and occluding them.

As for the Eagle Ford (**Figure 7**) pre-reaction sample (top row), we note a carbonate-rich matrix (green), clay platelets (pink), carbonate grains aggregated together (cyan), organic matter (blue), pyrite (red) dispersed across the matrix, and a few large micro-cracks running parallel to bedding. Looking at post-reaction images (bottom row), infilling of initial micro-cracks by barite precipitates is evident (bottom middle), while the majority of the carbonate grains have been dissolved by the fracture fluid, resulting in secondary porosity across the shale matrix.

Results from our permeability measurements show that shale mineral composition is a main factor to consider when reacting with the fracture fluid and subsequently affecting post-reaction permeability. In the case of the Marcellus microcore, the clay-rich sample exhibits a permeability reduction post-reaction to the fracture fluid. This reduction can be explained by the presence of barite precipitates, as seen in the EDS object classification images, being deposited into the micro-cracks and blocking the main transport pathways for flow across the sample. Even though the fracture fluid is a dissolution-favored solution, there is no observable secondary porosity generated in the Marcellus microcore.

In contrast to this behavior, the carbonate-rich Eagle Ford microcore, had an order of magnitude increase in intrinsic permeability, which we infer to be predominantly from calcite dissolution, leading to the creation of secondary porosity across the whole microcore surface in contact with the solution. The observed secondary porosity generation alone cannot explain the increase in permeability but suggests our ongoing hypothesis needs to look at the pore interconnectivity across the sample. In order to test our hypothesis, we would need to acquire high resolution µCT measurements set at a spatial resolution of 500nm before and after reaction to show the pore size changes and measurements highlighting the connectivity of pore bodies (future work outside of the scope of this project). Even though barite scale was observed as deposits in micro-cracks, the extent of carbonate dissolution apparently was far greater than that of barite precipitation. Looking back at the overarching model we propose in Figure 1, where we describe the chemical interactions with the shale matrix to be a series of static processes (*i.e.*, dissolution followed in time by precipitation), we note from our permeability results and supported EDS analysis, that the chemical interaction with the shale matrix is a dynamic process involving both dissolution and precipitation mechanisms at the same time but at different time scales. This hypothesis warrants further investigation of the reaction parameters and variability of the fracture fluid chemical compositions that can aid in the generation of dissolution-favored

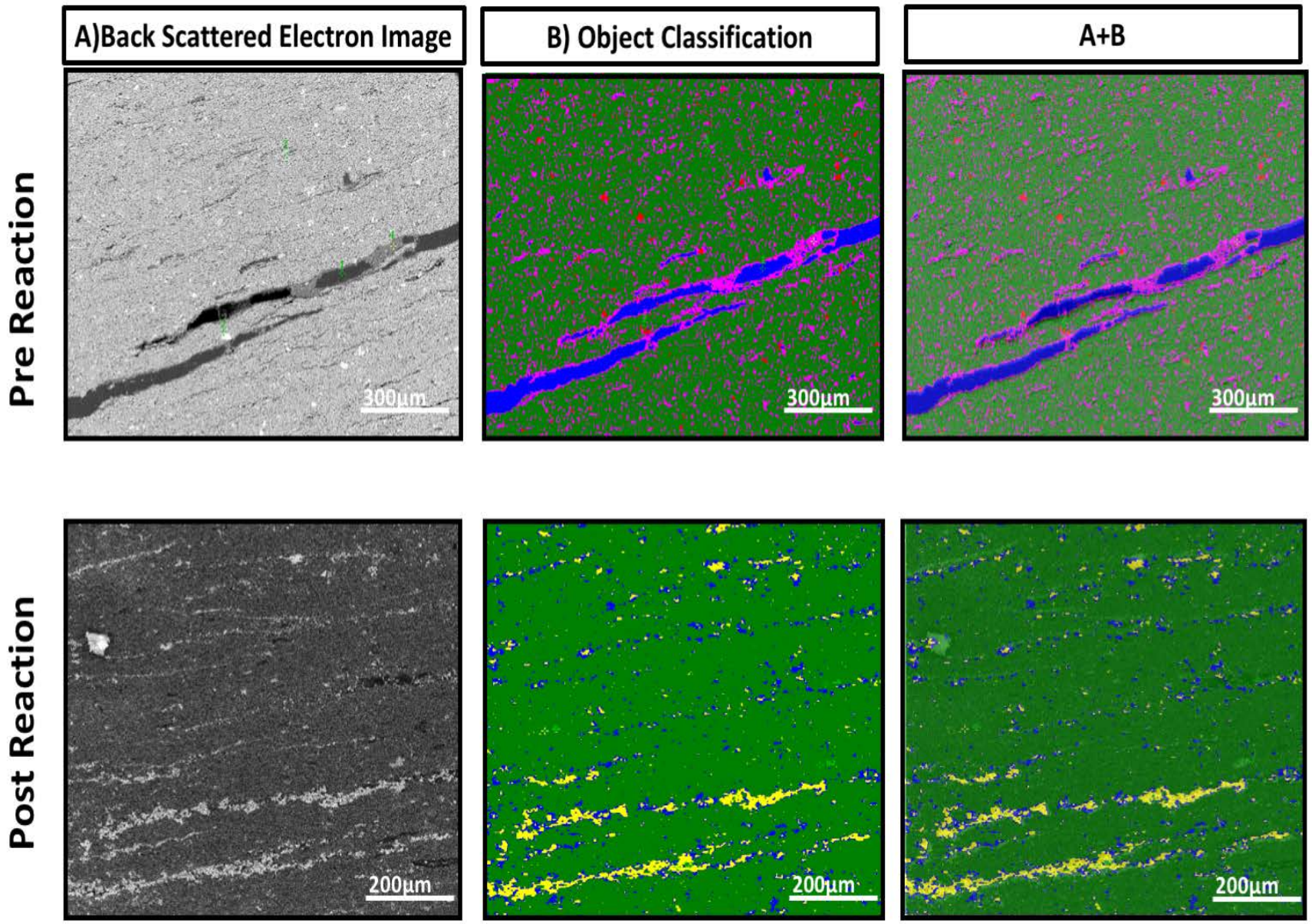

Figure 6. SEM and EDS images for Marcellus pre- (top row) and post-reaction (bottom row) to fracture fluid. Backscattered electron (CBS-a) images emphasize the shale texture and microcracks across the sample (left). The middle column shows object classification derived from EDS cluster analysis. From the overlay of both images (right), we note the barite precipitates deposited into the microcracks as a result of the fracture fluid reaction. Green: shale matrix; Blue: organic matter; Pink: clay enriched; Cyan: carbonate; Red: pyrite (red); Yellow: barite.

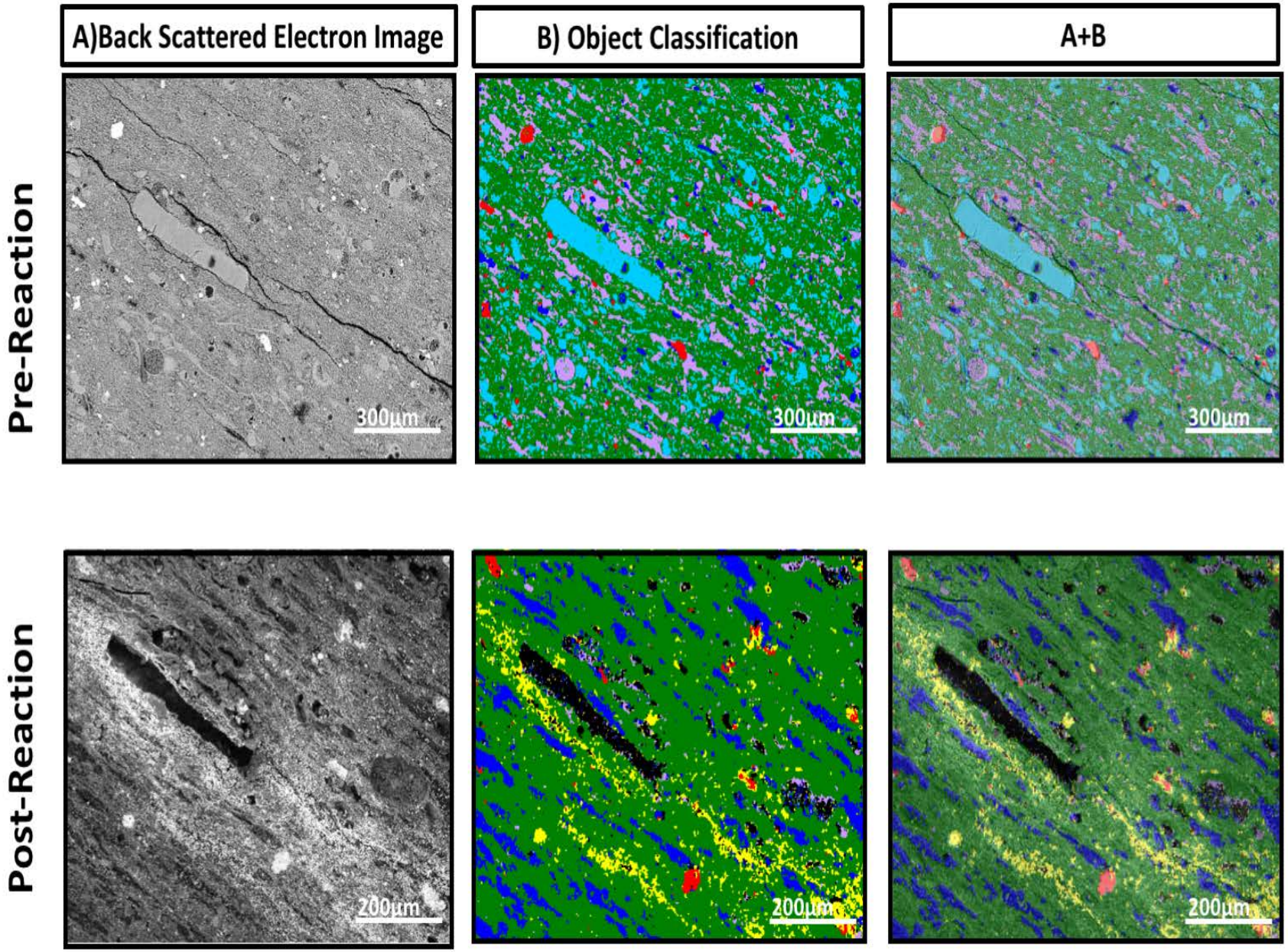

Figure 7 SEM and EDS images for Eagle Ford pre- (top row) and post-reaction (bottom row) to fracture fluid. Backscattered electron (CBS-a) images emphasize the shale texture and microcracks across the sample (left). The middle column shows object classification derived from EDS cluster analysis. From the overlay of both images (right), we note the barite precipitates deposited into the microcracks, with secondary porosity generation (black regions) due to the dissolution of carbonates. Green: shale matrix; Blue: organic matter; Pink: clay enriched; Cyan: carbonate; Red: pyrite (red); Yellow: barite.

reactions, while minimizing barite precipitation over time in our case, such that well production is enhanced over the long term.

Planned Experiments in the next quarter:

- Pore size characterization from fluid penetration measurements (Helium Pycnometry, Nitrogen Low Pressure Adsorption, and Mercury Porosimetry to contrast pre- and post-reaction alterations to pore volumes and sizes.

Manuscript Plans for Tasks 3&4(b).

URTeC 2018 extended abstract has been submitted and accepted "Effects of Hydraulic Fracturing Fluid Chemistry on Shale Matrix Permeability"

Task 3&4 (c): Reactive transport modeling of shale-fluid interactions

In earlier quarters, we set up a 1-D reactive transport model to try to simulate shale-fluid interactions. However, the chemical reaction framework in this preliminary model is too uncertain to depict the shale matrix alteration. Therefore, we first aimed to find the rates of two major reactions – barite precipitation and Fe(II) oxidation – using modeling tools. This approach will enable us to improve the reactive transport model for shale matrix reaction with more confidence. Data needed for this purpose were produced in earlier quarters of this project and were reported in Annual reports in 2016 and 2017 and published in Harrison *et al.* (2017) [6] and in Jew *et al*, (2017) [8].

Progress in Quarter 6:

Table 4. Objectives in Tasks 3&4 (c) for Quarter 6

Goal	Status
Obtain kinetics for barite precipitation from existing experimental data	Complete
Obtain kinetics for Fe(II) oxidation catalyzed by bitumen from existing data	Complete

Results in Quarter 6:

Barite precipitation

Batch reactors were used for barite precipitation over a one-week period at 80 ^{o}C as described in earlier quarterly reports in **Task 2**. Aqueous concentrations of $BaCl_2$ and Na_2SO_4 were both initially set at 0.1 mM with pH = 7. As barite precipitated, total measured Ba concentrations decreased at different rates depending on the organic or inorganic parameter tested. The results show that barite precipitation was fastest at pH > 5, with inhibition ~pH = 2 and lower.

Numerical modeling was carried out with the software package CrunchTope designed for simulating reactive transport systems in saturated porous medium [9]. The software can also model aqueous speciation, kinetic reactions, and fluid transport. For barite precipitation in a batch system, a single grid cell in the model was used, with volume fraction of aqueous phase ~ 100% (i.e., porous medium contains negligible solid phase of barite).

The barite precipitation reaction is expressed as:

$$Ba^{2+} + SO_4^{2-} \rightarrow BaSO_4(\text{barite}).$$ Eq. 1

The solubility product K_{sp} for barite is calculated as $10^{-9.59}$ at 80 ^{o}C. The rate (mol of Ba or SO_4^{2-} /m^3 porous medium/s) expression is written as

$$\text{Rate} = A \cdot k \cdot \left(\frac{Q}{K_{sp}} - 1\right), \quad \text{Eq. 2}$$

where A is the reactive surface area for barite (m^2/m^3), k is the rate constant (mol/m^2 of barite surface area/s), and Q is the ion activity product $(Ba^{2+})(SO_4^{2-})$. The values for the saturation Q/K_{sp} were calculated with CrunchTope, and the parameters we need to obtain for barite precipitation kinetics are A and k. Because A and k are multiplied, we assume A is constant 1, and compile all the rate variation in the rate constant k. A positive rate indicates precipitation of barite, and a negative rate indicates dissolution.

After fitting the experimental data, we found that the simulated results best describe the barite precipitation rates with $\log_{10}k$ = -7.7. **Figure 8** Left Panel shows the comparison between experimental data and the modeling results for time-resolved Ba concentration as a function of pH. The modeling results capture the rate increase from pH 2 to pH 3. For pH 5 and pH 6, the modeling results for Ba concentrations at the end of the experimental time frame are higher than experiments which is likely due to pH-dependent K_{sp}'s that are not well-known and thus not considered. **Figure 8** Right Panel shows the comparison of initial precipitation rates from experiments and from modeling. The experimental initial rates are calculated using the theoretical starting Ba concentration (0.1 mM) and the concentration measured at 10 hours. The pH 2 initial rates should be close to 0 but is calculated higher because the experimental data showed fluctuation along reaction times. The quality of the experimental and modeling data fitting is acceptable for simulating barite in a reactive transport model.

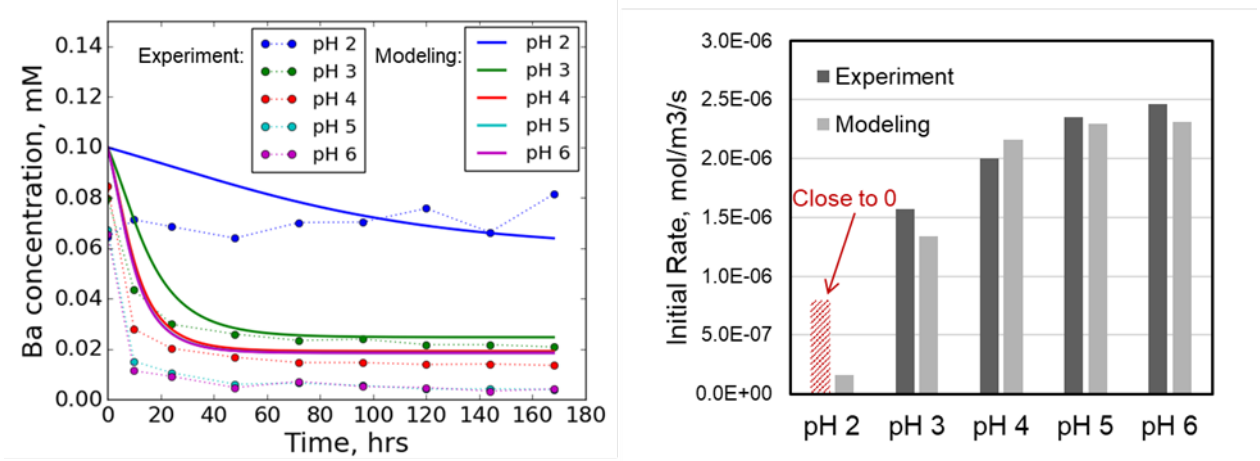

Figure 8. Comparison of experimental data and modeling results for time-resolved Ba concentration (Left) and initial precipitation rates (Right). See text for discussion.

Further analyses of water chemistry using CrunchTope indicate that the increase in the rate of barite precipitation from pH 2 to pH 3 corresponds to a change in speciation of sulfate anions. As shown in **Figure 9**, the sulfate anions are mostly in the form of HSO_4^- at pH 2, and switch to mostly SO_4^{2-} at pH 3 and higher. Therefore, the ion activity product $(Ba^{2+})(SO_4^{2-})$ increases significantly (by six-fold) when pH changes from 2 to 3. Consequently, the saturation Q/K_{sp} for

barite is higher, leading to faster precipitation. We can conclude that for the acidic pH range tested in the experiment, higher pH promotes barite precipitation by deprotonation of the bisulfate anion, resulting in higher concentration of sulfate anions, thus promoting barite precipitation.

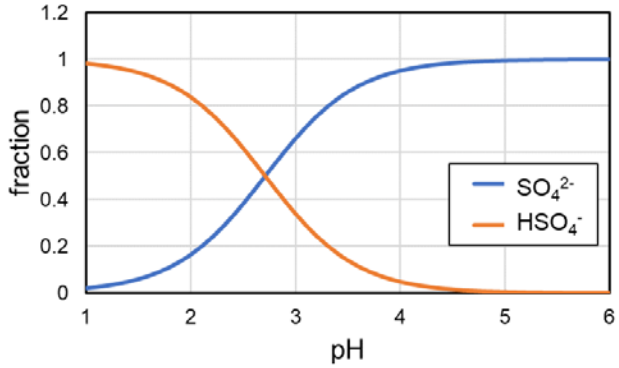

Figure 9. Predominance diagram of major oxidized S species, sulfate (SO_4^{2-}) and bisulfate (HSO_4^-) anion. These two species are in equal abundance at pH *ca* 2.6. Above this value, sulfate dominates.

Fe(II) oxidation catalyzed by bitumen

In the aqueous phase, Fe^{2+} is oxidized to Fe^{3+} by dissolved oxygen:

$$Fe^{2+} + H^+ + 0.25\ O_2(aq) \rightarrow\ Fe^{3+} + 0.5\ H_2O. \qquad \text{Eq. 3}$$

The product Fe^{3+} is then hydrolyzed to form Fe(III) (oxyhydr)oxides:

$$Fe^{3+} + 3H_2O \rightarrow 3H^+ + Fe(OH)_3 \rightarrow 3\ H^+ + 1.5H_2O + 0.5\ Fe_2O_3. \qquad \text{Eq. 4}$$

The overall reaction progress releases 2 H^+ for each Fe(II) oxidized and thus results in a decrease in solution pH.

During the first stage of this shale project, we found that Fe(II) oxidation is inhibited at low pH, but the presence of bitumen can override the pH inhibition effect, allowing Fe(II) oxidation at low pH. Batch experiments reported in Jew *et al*. (2017) show the effects of bitumen in aiding Fe(II) oxidation at low pH in the aqueous phase (**Figure 10**) [6].

CrunchTope was used to simulate the reaction system. The experimental results suggest that there are two pathways for Fe oxidation: In the absence of bitumen, the rate of Fe(II) oxidation is dependent on pH, and in the presence of bitumen, there is an additional oxidation pathway that is independent on pH but dependent on bitumen.

The pH-dependent rate law for reaction in **Eq. 5** is known from literature as:

$$\text{Rate} = k \cdot (\text{Fe(II)}) \cdot (O_{2(aq)}) \cdot (H^+)^{-2} \cdot \left(\frac{Q}{K_{eq}} - 1\right) \qquad \text{Eq. 5} \qquad [10]$$

where the rate constant k = 1.53 $\times 10^{-6}$ mol/kg of water/yr. Q and K_{eq} are the ion activity coefficient and equilibrium constant for **Eq. 5**, respectively. Positive rate means oxidation, and negative rate means reduction. Using only this pathway with literature values for k, we obtained

0 oxidation for the system with initial pH of 2, and 15% oxidation for the system with initial pH of 7, after 48 hours of reaction time.

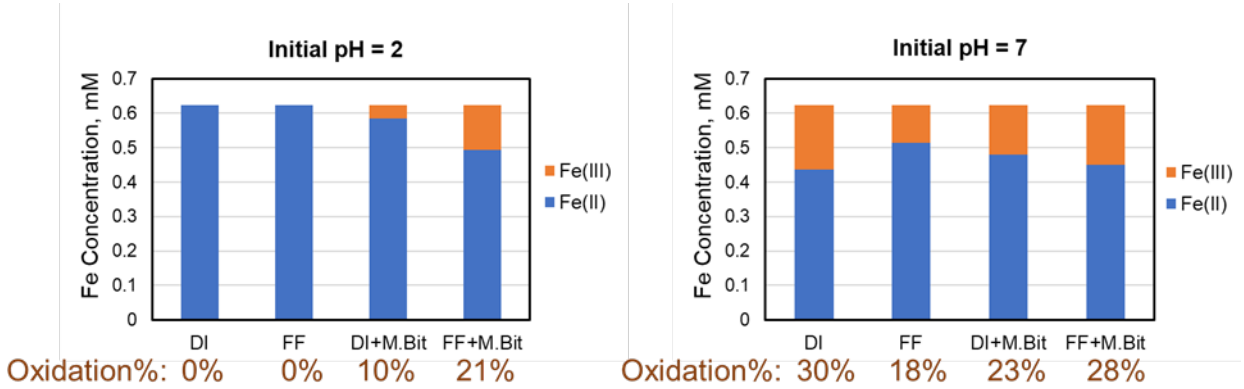

Figure 10. Oxidation of Fe(II) to Fe(III) at 48 hours. The reaction solution was either made from DI water or fracture fluid (FF). Bitumen extracted from Marcellus-NY (M.Bit) was added to examine the effect of bitumen.

The bitumen-dependent rate law is necessary to simulate Fe(II) oxidation in shale matrix and can be established by matching the modeling and experimental results. We express the reaction rate for this pathway as:

$$\text{Rate} = k \cdot (\text{Fe(II)}) \cdot (O_{2(aq)}) \cdot (\text{Bitumen})^{n} \cdot \left(\frac{Q}{K_{eq}} - 1\right). \qquad \text{Eq. 6}$$

The goal of matching the modeling results to experimental results is to obtain acceptable values for the rate constant k and the bitumen-dependent exponent n in **Eq. 6**. Fitting of the data resulted in $k = 8 \times 10^{5}$ mol/kgw/yr, and n = 0.1. The value for n is less than 1, which means that the reaction rate is sensitive to bitumen concentration when bitumen concentration is low. This initial conclusion is profoundly important because it indicates that only a small amount of bitumen is required in order to cause a qualitative change in Fe oxidation behavior. Since virtually all producing shales are relatively enriched in organics, *it is likely that organic-promoted oxidation pathways will always control Fe(II) oxidation and scale formation in unconventional reservoirs.*

This modeling work is currently in progress. Fine tuning of k and n in **Eq. 6** will be achieved in **Quarter 7** during simulation of shale sand experiments.

Combining the pH-dependent and bitumen-dependent rate expressions, we obtained the simulation results as shown in **Figures 11 and 12**, for initial pH 2 and 7 systems, respectively.

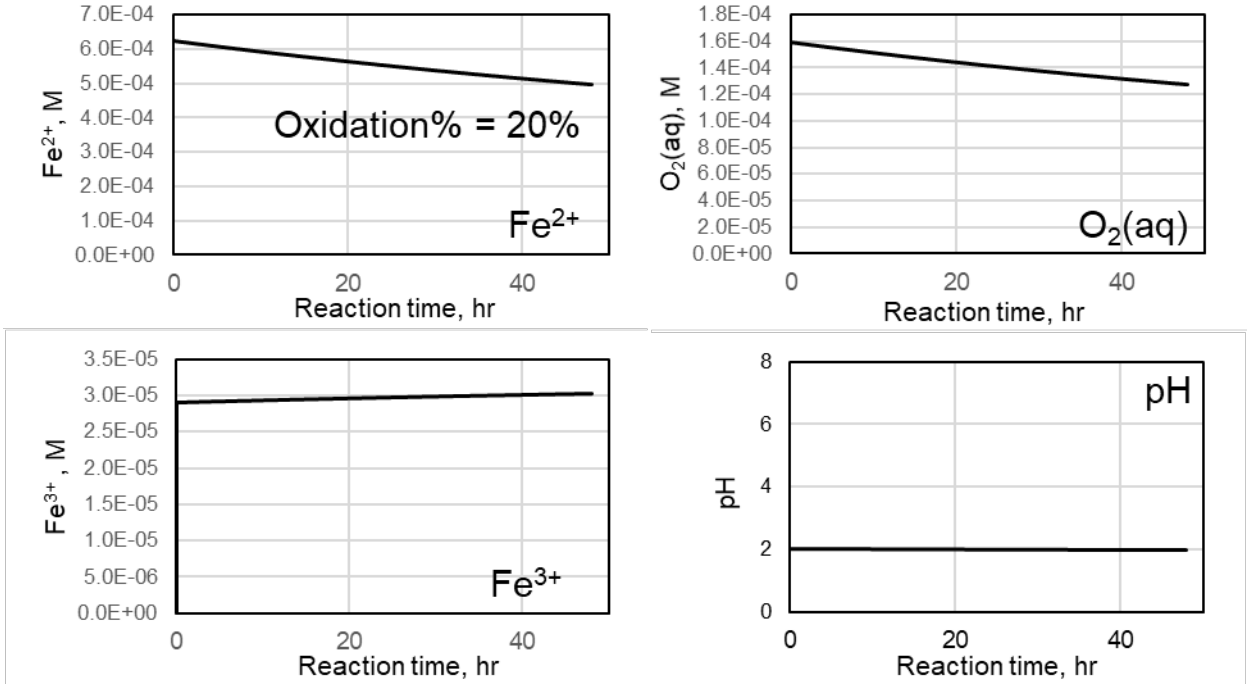

Figure 11. Modeling predictions for changes in Fe^{2+}, Fe^{3+}, pH and O_2 over time in the initial pH = 2 system.

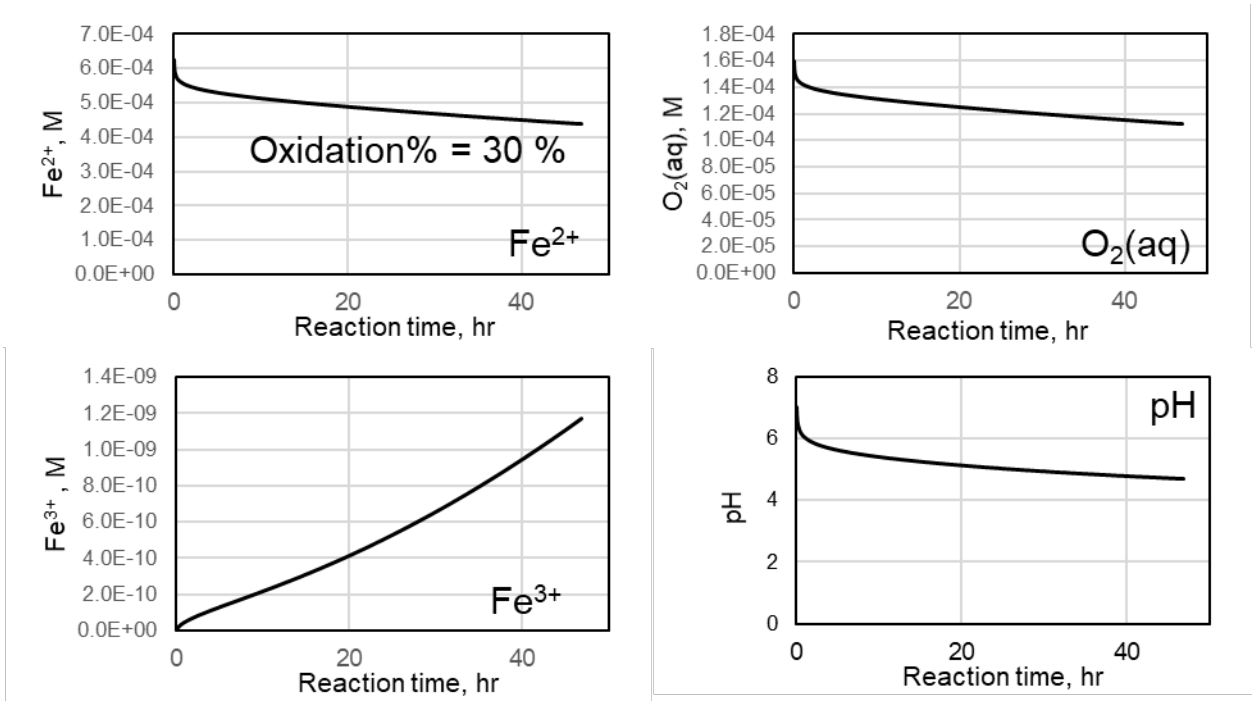

Figure 12. Modeling predictions for changing Fe^{2+}, Fe^{3+}, pH and O_2 for the initial pH = 7 system. As the reaction progresses pH drops, and the reaction slows due to the acid-inhibition effect on Fe(II) oxidation. Overall Fe^{3+} concentrations are lower than results in **Figure 11** due to Fe(III) precipitation, which removes Fe^{3+} from solution. (In contrast, Figure 13 plots the *total* amount of Fe, including precipitated Fe^{3+}.)

The simulations revealed several important points regarding the Fe(II) oxidation system:

- The consumption of dissolved oxygen is not significant and therefore does not reduce oxidation rate significantly within 48 hours.
- The reaction starting from pH 7 can quickly drop pH as the reaction product Fe^{3+} generates H^+ via hydrolysis. This pH drop slows down the reaction rate.
- The overall Fe(II) oxidation rate is not sensitive to the precipitation rate of Fe(III) (oxyhydr)oxides.
- Dissolution of atmospheric CO_2 into the reaction solution has a negligible effect on solution pH buffering capacity.
- Because ferrihydrite (amorphous Fe_2O_3 products formed when Fe^{3+} precipitates) can adsorb a small fraction of H^+ generated from Fe^{3+} hydrolysis the reaction rate of systems containing ferrihydrite will be slightly faster than a system without initial ferrihydrite.

Plans in the next quarter:

- Build batch reaction model for shale sand experiments and tune the rate constants for key chemical reactions. This model will incorporate the Fe(II) oxidation rate law obtained in this quarter.
- Build reactive transport model for shale matrix reactions. This model will incorporate both barite precipitation rate law and Fe(II) oxidation rate law obtained in this quarter.

Miscellaneous

An initial manuscript draft for the U portion of the project from the initial 2-year project has been completed and sent to co-authors for edits. This manuscript is entitled: The Effect of Hydraulic Fracturing Fluid on the Stability of Uranium in Unconventional Oil/Gas Shales. This article is targeted for publication in the journal Environmental Science & Technology.

References:

[1] Krauss, C. *Boom in American Liquefied Natural Gas Is Shaking Up the Energy World.* New Your Times Article, published Oct 16, 2017.

[2] Ghode, Roopali; Muley, Rajashree; Sarin, Rajkamal. *Operationally determined chemical speciation of barium and chromium in drilling fluid wastes by sequential extraction*. Chemical Speciation & Bioavailability, 7 (4) **1995**, 133-137.

[3] Neff, Jerry M. *US EPA Report: Fate and biological effects of oil well drilling fluids in the marine environment: A literature review*. **1981**, 1-178.

[4] Neff, Jerry M. *Estimation of bioavailability of metals from drilling mud barite*. Integrated Environmental Assessment and Management. 4 (2) **2008**, 184-193.

[5] Renock, Devon; Landis, Joshua D.; Sharma, Mukul. *Reductive weathering of black shale and release of barium during hydraulic fracturing*. Applied Geochemistry, 65, **2016**, 73-86.

[6] Jew, A. D.; Dustin, M. K.; Harrison, A. L.; Joe-Wong, C.; Thomas, D. L.; Maher, K.; Brown, Jr. G.E.; Bargar, J. R., *Importance of pH, Oxygen, and Bitumen on the Oxidation and Precipitation of Iron during Hydraulic Fracturing of Oil/Gas Shales*. Energy & Fuels 31(4), **2017**, 3643–3658. **DOI:** 10.1021/acs.energyfuels.6b03220

[7] Klinkenberg, L.J. *The permeability of porous media to liquids and gases.* Drilling and production practice. American Petroleum Institute, **1941**.

[8] Harrison, A. L., Jew, A. D., Dustin, M. K., Thomas, D. L., Joe-Wong, C. M., Bargar, J. R., Natalie Johnson, Brown, Jr., G.E., Maher, K. *Element release and reaction-induced porosity alteration during shale-hydraulic fracturing fluid interactions*. Applied Geochemistry, 82, **2017**, 47-62.

[9] Steefel, C. I. "CrunchFlow. Software for Modeling Multicomponent Reactive Flow and Transport. User's Manual."

[10] Stumm, Werner, and James J. Morgan. *Aquatic chemistry: chemical equilibria and rates in natural waters.* Vol. 126. John Wiley & Sons, 2012.

4. RISK ANALYSIS

Task 1: No significant risks to report

Task 2: No significant risks to report

Task 3&4. Understand fundamental precipitation and dissolution reactions in shale cores and determine shale matrix permeability changes by these reactions

Technical risks:

Risk 1. Shale matrix has very low permeability and takes long time to give response to a pressure pulse on the up-stream, thus may significantly increase our measurement time.

Mitigation:

(i) Risk 1. Permeability tests take a long time.

Mitigation: Several steps are being implemented: (a) Strategically identify a minimal set of cores required to establish scientific result; (b) Implement a single workflow that minimizes procedural steps during the pulse decay measurement, which enables longer times for cores to respond to pressure pulses during each step; (c) Use 1 inch-diameter cores because they have higher permeability than micro-cores (and hence faster measurement time); (d) React cores with fracture fluid 'off line' and bring them to the core-flood apparatus only to measure permeability (*i.e.*, do not use the permeameter apparatus to react cores with fracture fluid); and (e) Purchase additional pumps and core holders to expand experimental facility availability.

5. MILESTONE STATUS

Activity and milestones	Verification method†	Planned Milestone Date	Actual completion or status
Task 1. Project management			
1.1 Development of PMP	D	10-31-16	10-28-16
1.2 Recruit postdoc / RA	D	4-30-17	10-30-17
1.3 Quarterly research performance reports	D	1-30-17‡	7-30-17
1.4 Annual research performance report	D	11-30-17*	11-30-17
1.5 Final technical report	D	11-30-18	
Task 2. Influence of dissolved organic compounds on precipitate formation/stability			
2.1 Research/evaluation of literature and detailed experimental design	D	1-30-17	12-23-16
2.2 Set-up and test stirred tank reactors	D	1-30-17	12-19-16
2.3 Complete initial scoping experiments to determine types of organic compounds for detailed measurement	D	4-30-17	3-13-17
2.4 Complete measurements of initial rates of solid precipitation	D	7-30-17	6-30-17
2.5 Identification of precipitate mineralogy	XRD, XAS, SEM	10-30-17	9-30-17
2.6 Complete measurement of shale sand dissolution	D	7-30-17	6-30-17
2.7 Complete solubility measurements	D	7-30-17	10-30-17
2.8 Dissolution rate measurements in presence of shale sands with coupled dissolution and precipitation	D	10-30-17	10-30-17
2.9 Complete initial draft of manuscript	D	4-30-18	4-30-18
2.10 Submit manuscript	D	7-30-18	
Task 3. Impact of secondary pore networks on gas transport across shale matrix-fracture interfaces			
3.1 Research/evaluation of literature and design experiments favorable for secondary porosity generation	D	1-30-17	12-21-16
3.2 Submit beam time proposals	D	1-30-17	12-1-16
3.3 Acquire shale samples	D	1-30-17	11-9-16
3.4 Conduct telecons quarterly (as needed) with NETL group	N	1-30-17‡	Ongoing
3.5 Conduct telecons quarterly (as needed) with LANL group	**N**	1-30-17‡	Ongoing
3.6 Mineralogical characterization of shale samples	XRD, SEM	7-30-17	6-30-17
3.7 Measure gas permeability of unreacted cores	P	7-30-17	7-30-17
3.8 Collect μ-CT images for unreacted shale cores	μ-CT	7-30-17	3-7-17
3.9 Complete image processing for unreacted shale cores	D	10-30-17	10-30-17
3.10 Set up and test whole-core reactors: initial scoping experiments	D	7-30-17	11-30-16
3.11 Perform shale whole-core reactions	D	1-30-18	12-19-16
3.12 Collect μ-CT images on reacted cores	μ-CT	4-30-18	12-30-17
3.13 Collect XRM maps on thin section of unreacted and reaction cores	XRM, SEM	4-30-18	4-30-18
3.14 Measure gas permeability through reacted cores	P	4-30-18	4-30-18
3.15 Complete image processing and data analysis for reacted cores	D	9-30-18	In progress
3.16 Develop a shale sand batch reaction model to refine rate constants for new Fe(II) oxidation rate law	D	7-30-18	In progress
3.17 Complete initial draft of manuscript	D	9-30-18	In progress
3.18 Submit manuscript	D	12-31-18	

Activity and milestones	Verification method[†]	Planned Milestone Date	Actual completion or status
Task 4. Impact of secondary precipitation on gas transport across shale matrix-fracture interfaces			
4.1 Research/evaluation of literature and design experiments favorable for secondary precipitation	D	1-30-17	12-21-16
4.2 Measure gas permeability of unreacted cores	P	7-30-17	7-30-17
4.3 Collect μ-CT images on unreacted shale cores	μ-CT	7-30-17	3-7-17
4.4 Complete image processing and analysis on unreacted shale cores	D	10-30-17	10-30-17
4.5 Set up and test whole-core reactors: initial scoping experiments	D	10-30-17	3-20-17
4.6 Perform shale whole-core reactions	D	4-30-18	4-30-18
4.7 Measure permeability of reacted cores	D	9-30-18	3-30-18
4.8 Collect μ-CT images on reacted cores	P, μ-CT	10-31-18	3-30-18
4.9 Collect XRM maps on thin section of unreacted and reaction cores	XRM, SEM	10-31-18	In progress
4.10 Complete image processing and data analysis for reacted cores	D	3-31-19	
4.11 Develop a batch reaction model to refine rate constants for barite scale precipitation reactions	D	10-31-18	3-30-18
4.12 Build a 1D reactive transport model for shale matrix-fluid interface reactions	D	12-31-18	In progress

[‡] Quarterly reports will follow every 3 months following starting date. * Annual reports are due every 12 months on Nov 30.

[†] Verification Method Key:

AF = Software for data processing and visualization (Avizo Fire)
D = Documentation or data
EELS = Electron energy loss spectroscopy
FIB-SEM = Focused ion beam – scanning electron microscopy
μ-CT = Micrometer-scale X-ray computed tomography
nano-CT= Nanometer-scale X-ray computed tomography
N = Note from meeting
NM = Numerical modeling
OP = Optical petrography
P = Pulse-decay permeability
SAXS = Small angle X-ray scattering
SANS = Small angle neutron scattering
SEM = Scanning electron microscopy
TEM = Transmission electron microscopy
TXMWiz = Software for data processing of transmission X-ray images (TXM Wizard)
XAS = X-ray absorption spectroscopy
XRM = X-ray microprobe
XRD = X-ray diffraction

6. SCHEDULE STATUS

All milestones for this quarter have been met. As of the time of writing, the project is on-schedule.

Future changes to schedule and milestones: Qingyun Li (postdoc) will take a 2-month maternity leave from mid-June to mid-August. Since Qingyun is performing tasks 3&4(a) and (c), we will need to reschedule the remaining uncompleted subtasks. Specific changes are noted below.

During the first year of the current 2-year project, we discovered that transport along micro-fractures and reactions within these features appear to dominate the reactivity of the altered zone. Developing a reactive transport model that captures both the physical and chemical complexity of these interfaces is beyond the scope of our original 1 dimensional conceptualization of interface chemical gradients. At the time of writing, time on the project is limited (6 months), and it is prudent to re-define the scope of the modeling task, already underway. We are therefore planning to reprioritize subtasks 3.16 and 4.11, which are numerical modeling activities, to focus on the following three objectives that are strategically important to advancing the planned LBNL- and LLNL-led inter-lab project, "A New Framework for Microscopic to Reservoir-Scale Simulation of Hydraulic Fracturing and Production":

- Develop a batch reaction model to refine rate constants for barite scale precipitation reactions using experimental data reported in Task 2.
- Develop a shale sand batch reaction model for existing shale sand experiment data that incorporates the new Fe(II) oxidation rate law, where bitumen leached out of shale catalyzes the reaction.
- Build a 1D reactive transport model for shale matrix-fluid interface reactions involving coupled dissolution and precipitation using the whole-core results from Task 3&4(a) with respect to carbonate dissolution, S and Fe oxidation, and barite precipitation as a validation data set and incorporating the new Fe(II) oxidation and barite precipitation rate laws.

These three new steps are enumerated as subtasks in the revised Milestones plan (Section 5) as detailed in the table below.

Modification explanation log for milestones list:

Task	Planned date	Revised date	New Task goal / Explanation
3.15	7-30-18	9-30-18	Accommodate 2-month maternity leave
3.16	7-30-18	9-30-18	Accommodate 2-month maternity leave New task name: "Develop a shale sand batch reaction model to refine rate constants for new Fe(II) oxidation rate law"
3.17	7-30-18	9-30-18	Accommodate 2-month maternity leave
3.18	10-31-18	12-31-18	Accommodate 2-month maternity leave
4.10	1-31-19	3-31-19	Accommodate 2-month maternity leave
4.11	10-31-18	NA	New task name: Develop a batch reaction model to refine rate constants for barite scale precipitation reactions
4.12	NA	12-31-18	New task: Build a 1D reactive model for shale matrix-fluid interface reactions

Project timeline from the Project Management Plan.

Task	Title	Month of project																												
		2016			2017												2018												2019		
		1	2	3	4	5	6	7	8	9	10	11	12	13	14	15	16	17	18	19	20	21	22	23	24	25	26	27	28	29	30
		Oct	Nov	Dec	Jan	Feb	Mar	Apr	May	Jun	Jul	Aug	Sep	Oct	Nov	Dec	Jan	Feb	Mar	Apr	May	Jun	Jul	Aug	Sep	Oct	Nov	Dec	Jan	Feb	Mar
1	**Project management plan**																														
1.1	Development of PMP																														
1.2	Recruit postdoc/RA																														
1.3	Quarterly research performance reports																														
1.4	Annual research performance report																														
1.5	Final technical report																														
2	**Influence of dissolved organic compounds on precipitate formation/stability**																														
2.1	Evaluate literature/ experimental design																														
2.2	Set-up and test stirred tank reactors																														
2.3	Complete initial scoping experiments																														
2.4	Complete measurements of initial rates of solid precipitation																														
2.5	Identification of precipitate mineralogy																														
2.6	Measure shale sand dissolution																														
2.7	Complete solubility measurements																														
2.8	Dissolution rate measurements in presence of shale sands																														
2.9	Complete initial draft of manuscript																														
2.10	Submit manuscript																														
3	**Impact of secondary pore networks on gas transport across shale matrix-fracture interfaces**																														
3.1	Evaluate literature/ experimental design																														
3.2	Submit beam time proposals																														
3.3	Acquire shale samples																														
3.4	Quarterly (as needed) with NETL group																														
3.5	Quarterly (as needed) with LANL group																														
3.6	Mineral characterization shale samples																														
3.7	Measure permeability of unreacted cores																														
3.8	Collect μ-CT images, unreacted cores																														
3.9	Image processing, unreacted shale cores																														
3.10	Test whole-core reactors: Initial scoping experiments																														
3.11	Perform shale whole-core reactions																														
3.12	Collect μ-CT images on reacted cores																														
3.13	XRM maps, unreacted/ reacted cores																														
3.14	Measure permeability of reacted cores																														
3.15	Image processing, reacted shale cores																														
3.16	Develop a batch reaction model to refine rate constants for Fe(II) oxidation																														
3.17	Complete initial draft of manuscript																														
3.18	Submit manuscript																														
4	**Impact of matrix precipitation on gas transport across shale matrix-fracture interfaces**																														
4.1	Evaluate literature/ experimental design																														
4.2	Measure permeability of unreacted cores																														
4.3	Collect μ-CT images, unreacted cores																														
4.4	Image processing, unreacted shale cores																														
4.5	Test whole-core reactors: Initial scoping experiments																														
4.6	Perform shale whole-core reactions																														
4.7	Measure permeability of reacted cores																														
4.8	Collect μ-CT images on reacted cores																														
4.9	XRM maps, unreacted/ reacted cores																														
4.10	Image processing, reacted shale cores																														
4.11	Develop a batch reaction model to refine rate constants for barite scale																														
4.12	Build a 1D reactive model for shale matrix-fluid interface reactions																														

7. COST STATUS

Cost Plan/Status										
Basesline Reporting Quarter		Year 4	Start: 10/1/16 End: 9/30/17			Year 5	Start: 10/1/17 End: 9/30/18			
		Q1	Q2	Q3	Q4	Q5	Q6	Q7	Q8	
Baseline Cost Plan										
Federal Share	Task 1	$ 9,686	$ 9,686	$ 9,686	$ 9,686	$ 12,750	$ 12,750	$ 12,750	$ 12,750	
	Task 2	$ 31,681	$ 31,681	$ 31,681	$ 31,681	$ 44,625	$ 44,625	$ 44,625	$ 44,625	
	Task 3	$ 42,400	$ 42,400	$ 42,400	$ 42,400	$ 35,700	$ 35,700	$ 35,700	$ 35,700	
	Task 4	$ 23,733	$ 23,733	$ 23,733	$ 23,733	$ 34,425	$ 34,425	$ 34,425	$ 34,425	
	Task 5									
	Task 6									
Non-Federal Share										
Total Planned Costs (Federal and Non-Federal)										
Cumulative Baseline Cost		$ 107,500	$ 215,000	$ 322,500	$ 430,000	$ 557,500	$ 685,000	$ 812,500	$ 940,000	
Actual Incurred Costs										
Federal Share	Task 1	$ 7,290	$ 13,437	$ 8,509	$ 16,530	$ 14,370	$ 9,979			
	Task 2	$ 25,514	$ 47,028	$ 29,782	$ 57,855	$ 50,294	$ 34,927			
	Task 3	$ 20,411	$ 37,622	$ 23,826	$ 46,284	$ 40,236	$ 27,942			
	Task 4	$ 19,682	$ 36,279	$ 22,975	$ 44,631	$ 38,799	$ 26,944			
	Task 5	$ -	$ -	$ -	$ -	$ -	$ -	$ -	$ -	
	Task 6	$ -	$ -	$ -	$ -	$ -	$ -	$ -	$ -	
Non-Federal Share										
Total Incurred Costs - Quarterly (Federal and Non-Federal)										
Cumulative Incurred Cost		$ 72,898	$ 134,366	$ 85,093	$ 165,300	$ 143,698	$ 99,792	$ -	$ -	
Variance										
Federal Share	Task 1	$ 2,396	$ (3,750)	$ 1,177	$ (6,843)	$ (1,620)	$ 2,771	$ 12,750	$ 12,750	
	Task 2	$ 6,167	$ (15,347)	$ 1,899	$ (26,174)	$ (5,669)	$ 9,698	$ 44,625	$ 44,625	
	Task 3	$ 21,988	$ 4,777	$ 18,574	$ (3,884)	$ (4,536)	$ 7,758	$ 35,700	$ 35,700	
	Task 4	$ 4,050	$ (12,546)	$ 758	$ (20,898)	$ (4,374)	$ 7,481	$ 34,425	$ 34,425	
	Task 5	$ -	$ -	$ -	$ -	$ -	$ -	$ -	$ -	
	Task 6	$ -	$ -	$ -	$ -	$ -	$ -	$ -	$ -	
Non-Federal Share		$ -	$ -	$ -	$ -	$ -	$ -	$ -	$ -	
Total Variance - Quarterly (Federal and Non-Federal)		$ -	$ -	$ -	$ -	$ -	$ -	$ -	$ -	
Cumulative Variance		$ 52,503	$ 25,637	$ 48,044	$ (9,755)	$ (25,953)	$ 1,755	$ 129,255	$ 256,755	

8. Collaborative Leveraging: We are currently collaborating with 1 Ph.D. student in the Zoback research group as well as 1 Ph.D. student in the Kovscek research group at Stanford University. Additional, collaboration is ongoing with the Hakala and Lopano groups at NETL. A new LDRD proposal has been submitted that would support the development of machine learning algorithms for accelerating segmentation of synchrotron μ-CT image data. If successful, this activity will strongly support the existing NETL project.

9. CONCLUSIONS

For the whole-core experiments, we quantified the reaction depth of secondary Fe(III) precipitation in the altered zone as 200 to 300 μm for both Pennsylvania Marcellus and Eagle Ford shales. The overall reaction depth is slighter larger for Eagle Ford shale compared to the Pennsylvania Marcellus. These secondary precipitates were not confined to micro-cracks but formed a 1D profile perpendicular to the shale-fluid interface, indicating that the shale matrix could be chemically reactive even in zones absent of micro-cracks. This work shows that, when present in fracture fluid, oxygen penetrates rapidly into unmicro-fractured shale interfaces (the 3-week time frame for these experiments is well within the typical 3- to 6-week duration of shut-in periods during stimulation and development). These findings provide an important perspective on alteration of shale matrices and fracture surfaces, *i.e., that "low reactivity" shale matrices are, in fact, quite reactive*.

Permeability analyses showed a major difference between the response of siliceous Marcellus and carbonate-rich Eagle Ford to reaction with fracture fluid for 6 days of reaction. Barite was actively precipitating and filling micro-cracks in both shales. Moreover, because barite precipitation rates are strongly promoted at near-neutral pH (which is found in carbonate-rich shale), the extent of barite precipitation is substantially greater in Eagle Ford shale than in the Marcellus samples. Consequently, these new results indicate that an alternative mechanism (*i.e.*, other than scale precipitation) must be operating that can allow permeability to improve. Looking back to **Figure 1**, it can be appreciated that dissolution must be considered. Forensic analyses of the sacrificed permeability core samples strongly suggest that dissolution of carbonate grains continued in parallel with or even *after* barite scale precipitation was complete. These results have several profound implications for our research program and for shale reservoir management in general. On one hand, they indicate that our original process model (*cf.*, **Figure 1**; also see the 2017 Annual report), which implicitly invokes two distinct chemical states of the shale-fluid system (*i.e.*, dissolution-favorable and precipitation-favorable) separated in time, must be modified. The updated conceptual model must allow for dynamic process mixing, with matrix dissolution and scale precipitation co-occurring at different locations in the systems at micro-fracture and pore scales.

On the other hand, the current findings also emphasize the importance of the *rates* of these two different processes (dissolution and precipitation). That is to say, these results show us a path to engineer the permeability of the altered zone at shale-fluid interfaces *if we have the ability to manipulate scale precipitation and matrix dissolution rates*. Our work over the past two years has shown that the rates of both processes are highly sensitive to pH, ionic strength, and the presence of dissolved solutes such as sulfate. Consequently, we find ourselves well positioned to design and launch a focused new research activity (in the FY19 period) that could design and test chemical-based methods to engineer altered zone permeability by manipulating the rates of dissolution and precipitation reactions.

In Task 3&4 (c), kinetic chemical modeling was carried out for barite precipitation as a function of pH and for aqueous Fe(II) oxidation catalyzed by bitumen. By matching the modeling results with experimental data, important rate constants were obtained. The Ba precipitation results also show that the precipitation rate is enhanced by high pH because increasing pH fully deprotonates the bisulfate anion to SO_4^{2-} increasing the saturation index for barite. The Fe(II) oxidation results show that *two* pathways are required for Fe(II) oxidation to Fe(III). One is the pH-dependent pathway (Eq. 3), in which the rate is inversely dependent on H^+ concentration, and the other is the bitumen-dependent pathway (Eq. 6) that enables oxidation of Fe(II) to Fe(III) even when pH is low. These conclusions are also profoundly important for shale reservoir management because they indicate that only a small amount of bitumen is required in order to cause a qualitative change in Fe oxidation behavior. Since virtually all economically important shales are relatively enriched in organics, it is likely that before injected fluid is neutralized by mineral dissolution, *organic-promoted oxidation pathways will control Fe(II) oxidation and scale formation in all unconventional reservoirs.*

APPENDIX A. Deliverables during the current fiscal year

Manuscripts.

URTeC Extended Abstracts (In Press):

1. *Barium Sources in Hydraulic Fracturing Systems and Chemical Controls on its Release into Solution*. Adam D. Jew, Qingyun Li, David Cercone, Kate Maher, Gordon E. Brown, Jr., John R. Bargar
2. *Imaging Pyrite Oxidation and Barite Precipitation in Gas and Oil Shales*. Qingyun Li, Adam D. Jew, Andrew M. Kiss, Arjun Kohli, Abdulgader Alalli, Anthony R. Kovscek, Mark D. Zoback, David Cercone, Katharine Maher, Gordon E. Brown, Jr., John R. Bargar
3. *Effects of hydraulic fracturing fluid on shale matrix permeability*. Abdulgader Alalli, Qingyun Li, Adam Jew, Arjun Kholi, John R. Bargar, Mark Zoback

Environmental Science & Technology (In Review):

4. *Shale Kerogen-Hydraulic Fracturing Fluid Interactions and Contaminant Release*. Megan K. Dustin, Adam D. Jew, Anna L. Harrison, Claresta Joe-Wong, Dana L. Thomas, Katharine Maher, Gordon E. Brown, Jr., John R. Bargar

Energy & Fuels (In Preparation):

5. *Organic and Inorganic Controls on Barite Precipitation in Hydraulic Fracturing Systems*. Adam D. Jew, Qingyun Li, Kate Maher, Gordon E. Brown, Jr., John R. Bargar

Environmental Science & Technology (In Preparation):

6. *The Effect of Hydraulic Fracturing Fluid on the Stability of Uranium in Unconventional Oil/Gas Shales*. Adam D. Jew, Clemence J. Besancon, Scott J. Roycroft, Vincent S. Noel, Gordon E. Brown, Jr., John R. Bargar

Presentations at National Meetings.

7. AIChE Annual Meeting, Oct. 29-Nov. 3, 2017, Minneapolis, MN. Adam D. Jew, David Cercone, Qingyun Li, Megan K. Dustin, Anna L. Harrison, Claresta Joe-Wong, Dana L. Thomas, Kate Maher, Gordon E. Brown, Jr., John R. Bargar. *Chemical controls on secondary mineral precipitation of Fe and Ba in hydraulic fracturing systems.*
8. AGU Fall Meeting, Dec. 11-15, 2017, New Orleans, LA. Qingyun Li, Adam D. Jew, Gordon E. Brown, Jr., John R. Bargar. *Chemical reactivity of shale matrixes and the effects of barite scale formation*
9. DOE Upstream Workshop, Feb. 14, 2018, Houston, TX. Alexandra Hakala, Joe Morris, John Bargar, Jens Birkholzer. *Fundamental Shale Interactions-DOE National Laboratory Research*

URTeC Conference, July 23-25, 2018, Houston, TX:

10. Adam D. Jew, Qingyun Li, David Cercone, Kate Maher, Gordon E. Brown, Jr., John R. Bargar. *Barium Sources in Hydraulic Fracturing Systems and Chemical Controls on its Release into Solution*.
11. Qingyun Li, Adam D. Jew, Andrew M. Kiss, Arjun Kohli, Abdulgader Alalli, Anthony R. Kovscek, Mark D. Zoback, David Cercone, Katharine Maher, Gordon E. Brown, Jr., John R. Bargar. *Imaging Pyrite Oxidation and Barite Precipitation in Gas and Oil Shales*

12. Abdulgader Alalli, Qingyun Li, Adam Jew, Arjun Kholi, John R. Bargar, Mark Zoback. *Effects of hydraulic fracturing fluid on shale matrix permeability*.

Other activities.

- Participant in DOE-FE Oil and Natural Gas Knowledge Management adviser group (A. Jew)
- Participant in DOE-FE Oil and Natural Gas Science Leadership adviser group (J. Bargar)